Article

Galaxies in voids assemble their stars slowly

https://doi.org/10.1038/s41586-023-06109-1

Received: 16 May 2022

Accepted: 20 April 2023

Published online: 28 June 2023

Check for updates

Jesús Domínguez-Gómez[1]✉, Isabel Pérez[1,2], Tomás Ruiz-Lara[1,3], Reynier F. Peletier[3], Patricia Sánchez-Blázquez[4], Ute Lisenfeld[1,2], Jesús Falcón-Barroso[5,6], Manuel Alcázar-Laynez[1], María Argudo-Fernández[1,2], Guillermo Blázquez-Calero[7], Hélène Courtois[8], Salvador Duarte Puertas[1,7,9], Daniel Espada[1,2], Estrella Florido[1,2], Rubén García-Benito[7], Andoni Jiménez[1], Kathryn Kreckel[10], Mónica Relaño[1,2], Laura Sánchez-Menguiano[1,2], Thijs van der Hulst[3], Rien van de Weygaert[3], Simon Verley[1,2] & Almudena Zurita[1,2]

Galaxies in the Universe are distributed in a web-like structure characterized by different large-scale environments: dense clusters, elongated filaments, sheetlike walls and under-dense regions, called voids[1–5]. The low density in voids is expected to affect the properties of their galaxies. Indeed, previous studies[6–14] have shown that galaxies in voids are, on average, bluer and less massive, and have later morphologies and higher current star formation rates than galaxies in denser large-scale environments. However, it has never been observationally proved that the star formation histories (SFHs) in voids are substantially different from those in filaments, walls and clusters. Here we show that void galaxies have had, on average, slower SFHs than galaxies in denser large-scale environments. We also find two main SFH types present in all the environments: 'short-timescale' galaxies are not affected by their large-scale environment at early times but only later in their lives; 'long-timescale' galaxies have been continuously affected by their environment and stellar mass. Both types have evolved more slowly in voids than in filaments, walls and clusters.

In Fig. 1 we find that, on average, galaxies in voids assemble 50% and 70% of their stellar mass later than in filaments and walls by 1.03 ± 0.06 Gyr and 1.20 ± 0.05 Gyr, respectively, and much later than in clusters (by 1.91 ± 0.06 Gyr and 2.43 ± 0.05 Gyr). In addition, in Fig. 2, we find that the star formation histories (SFHs) at early times describe a bimodal distribution around this average in the three large-scale environments. We then classify the SFHs into two types: the short-timescale SFH (ST-SFH) is characterized by a high star formation (approximately 27% of the total stellar mass, the peak of the distributions) happening at the earliest time, while the long-timescale SFH (LT-SFH) has a star formation happening more uniformly over time. The distinction between these two types of SFHs allows us to evaluate the role of the large-scale environment in star formation, by comparing the shape of the SFHs and assembly times between all three large-scale environments and also by paying attention to the probability of finding each SFH type in voids, filaments and walls, and clusters (see Extended Data Fig. 1 for the exact shape of an example of an ST-SFH galaxy and an LT-SFH galaxy and the differences between them).

In Fig. 3, it can be seen that galaxies with ST-SFHs assembled, on average, 30% of their stellar mass at early times (approximately 12.5 Gyr ago) and decrease their star formation later in their lives. Galaxies with LT-SFHs, however, have assembled a lower stellar mass fraction (approximately 15%) at early times. By definition, ST-SFH galaxies assemble their stellar mass earlier than LT-SFH. It is more likely for a void galaxy to have a LT-SFH (51.7 ± 0.9%) than for those in filaments and walls (44.5 ± 0.3%) or clusters (36.1 ± 0.5%; see legends in Fig. 3). Galaxies with ST-SFHs, on average, assemble their stellar mass at similar rates in the three large-scale environments. Galaxies with LT-SFHs, on average, assemble 50% and 70% of their stellar mass more slowly in voids than in filaments and walls by 1.05 ± 0.09 Gyr and 0.86 ± 0.06 Gyr, respectively, and much more slowly than in clusters (by 2.38 ± 0.10 Gyr and 2.22 ± 0.07 Gyr). These might be the main reasons why we find in Fig. 1 that galaxies, on average, assemble their stellar mass later in voids than in denser large-scale environments. However, the stellar mass distributions of these galaxy samples depend on the large-scale environment[7] (galaxies in voids are, on average, less massive than galaxies in denser large-scale environments; see Extended Data Figs. 2 and 3) and it is necessary to test how these differences affect our results when carrying out further comparisons for a given stellar mass.

We then define three new subsamples with the same stellar mass distribution (see Methods 'Sample selection' for more details). In Fig. 4a,d we see that, regardless of their SFH type, cluster galaxies, on average, assemble their stellar mass faster than galaxies in voids and in filaments and walls at any given stellar mass, except for very high stellar masses, where galaxies assemble their stellar mass at the same time in all three large-scale environments. Low-mass and high-mass galaxies, on average, assemble 50% and 70% of their stellar mass at the same rate in voids as in filaments and walls. However, intermediate-mass galaxies assemble both 50% and 70% of their stellar mass later in voids than in filaments and walls.

In Fig. 4b, we find that galaxies with ST-SFHs, on average, have formed 50% of their stars very early (approximately 11 Gyr ago), independently of their large-scale environment and stellar mass. This suggests that, in the early Universe, the density contrasts between the upcoming

[1]Departamento de Física Teórica y del Cosmos, Universidad de Granada, Granada, Spain. [2]Instituto Carlos I de Física Teórica y Computacional, Universidad de Granada, Granada, Spain. [3]Kapteyn Astronomical Institute, University of Groningen, Groningen, The Netherlands. [4]Departamento de Física de la Tierra y Astrofísica & IPARCOS, Universidad Complutense de Madrid, Madrid, Spain. [5]Instituto de Astrofísica de Canarias, La Laguna, Spain. [6]Departamento de Astrofísica, Universidad de La Laguna, La Laguna, Spain. [7]Instituto de Astrofísica de Andalucía - CSIC, Granada, Spain. [8]Université Claude Bernard Lyon 1, IUF, IP2I Lyon, Villeurbanne, France. [9]Département de Physique, de Génie Physique et d'Optique, Université Laval, and Centre de Recherche en Astrophysique du Québec (CRAQ), Québec, Québec, Canada. [10]Astronomisches Rechen-Institut, Zentrum für Astronomie, Universität Heidelberg, Heidelberg, Germany. ✉e-mail: jesusdg@ugr.es

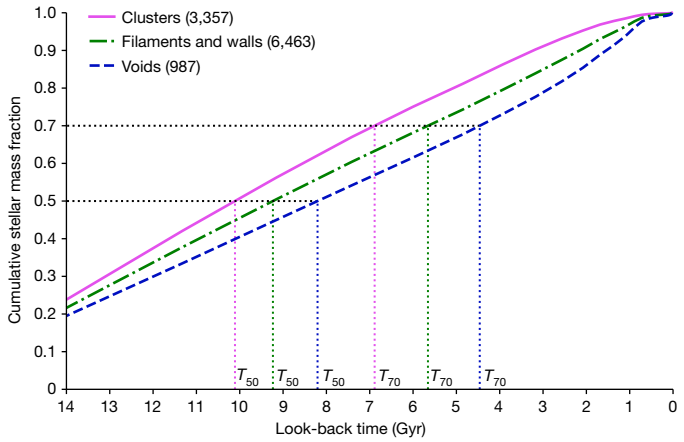

Fig. 1 | Average cumulative SFH. Cumulative stellar mass fraction formed at a given look-back time (in Gyr), for galaxies in voids (blue dashed line), filaments and walls (green dot-dashed line) and clusters (purple solid line). The used samples take into account the selection criteria applied by the quality control analysis and are based on different stellar mass distributions. As representative quantities of the stellar mass assembly rate, dotted lines depict the average assembly times of 50% (T_{50}) and 70% (T_{70}) of the stellar mass, for which we find that the differences in SFH are maximal. By definition, $T_{100} = 0$ Gyr means that the galaxy forms 100% of its stellar mass today and T_{70} and T_{50} are correlated, that is, if T_{50} is higher in a sample, then the T_{70} is also higher. In general, the standard error of the mean (1σ) is smaller than the line width of the curves. The number of galaxies is represented in the legend for each large-scale environment.

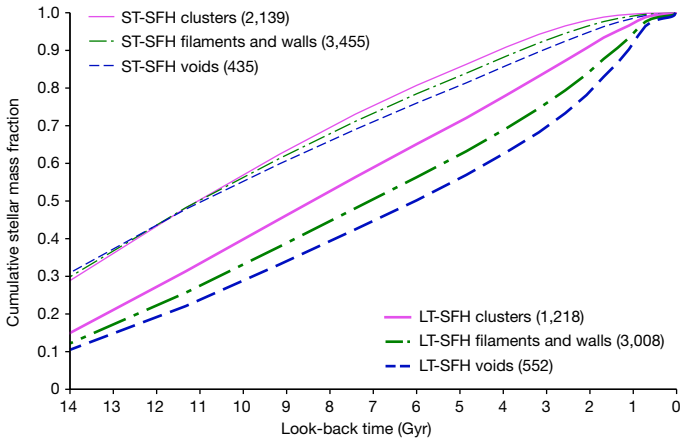

Fig. 3 | Two types of SFH. Cumulative stellar mass fraction formed at a given look-back time (in Gyr) for galaxies with ST-SFH (thin lines) and LT-SFH (thick lines), in voids (blue dashed lines), filaments and walls (green dot-dashed lines) and clusters (purple solid lines). The samples used take into account the selection criteria applied by the quality control analysis and are based on different stellar mass distributions. In general, the standard error of the mean (1σ) is smaller than the line width of the curves. The number of galaxies for each large-scale environment and SFH type is given in the legends.

large-scale environments were not strong enough to create a difference in the assembly rate between the galaxies that were forming at that time. The assembly time differences that we find for galaxies with ST-SFHs are only imprinted later on in their evolution (for example, T_{70}; see Fig. 4e), when the large-scale environment does play a role. Whereas galaxies in clusters with ST-SFH exhibit similar assembly times for any given stellar mass ($T_{70} \approx 8$ Gyr), void and filament and wall galaxies, at some point, slow down their evolution compared with cluster galaxies, more substantially at low stellar masses than at high stellar masses. This might indicate that low-mass galaxies with ST-SFHs were formed at early times as were their massive counterparts but have been later affected by the large-scale environmental density, which slowed down their SFH. However, at very low stellar masses, the number of galaxies (8, 24 and 9 galaxies) is less statistically significant than at higher stellar masses. High-mass galaxies with ST-SFHs have been less affected by their large-scale environment owing to early mergers (even in voids, whose galaxies are not necessarily isolated, as they can be found in groups and in mergers[11,15,16]) or the effect of more massive dark matter halos. Moreover, the fraction of ST-SFH low-mass galaxies (Extended Data Table 1) is much lower than the fraction of ST-SFH high-mass galaxies, which suggests that galaxies that were assembled quickly at the very beginning of the Universe (ST-SFH) are more likely to be massive galaxies now, to have gathered mass by consecutive mergers, to have more massive dark matter halos, to run out of gas and to quench.

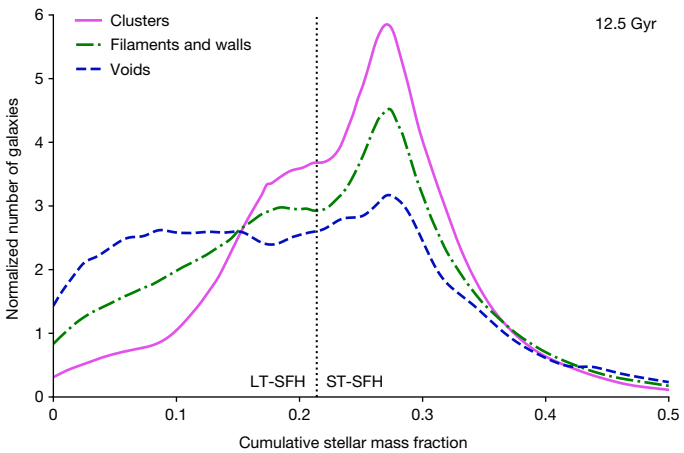

Fig. 2 | Bimodal distributions of the cumulative SFHs at 12.5 Gyr. Normalized number of galaxies versus the cumulative stellar mass fraction. The samples used take into account the selection criteria applied by the quality control analysis and are based on different stellar mass distributions. The SFHs are classified into ST-SFH or LT-SFH using the vertical dotted line at 21.4% of the stellar mass (relative minimum of the sample of galaxies in filaments and walls and the inflexion point of the sample of galaxies in clusters) as a classification criterion that splits the distributions into two areas which represent the probability of a galaxy having one of the SFH types in each large-scale environment.

Galaxies with LT-SFHs have assembled their stellar mass later than those with ST-SFHs by 1.09 Gyr to 5.88 Gyr depending on the large-scale environment, assembly time and stellar mass. This delay might have been enough for the LT-SFH to be affected by the large-scale environment since very early on, in contrast with the ST-SFH. We find, in Fig. 4c,f, that void galaxies with LT-SFHs evolve more slowly than galaxies in clusters at any given stellar mass and slightly more slowly than galaxies in filaments and walls at intermediate stellar masses. The evolution of cluster galaxies with LT-SFH is accelerated, at any given stellar mass, by the higher density and higher probability of undergoing interactions in their large-scale environment compared with voids and with filaments and walls. In the same way, galaxies in filaments and walls evolve faster than galaxies in voids, which indicates that evolution at later times is influenced by the large-scale structure, more substantially at intermediate stellar masses than at high and low stellar masses. At high stellar masses, galaxies might have been more affected by local interactions or their massive dark matter halos than by their large-scale environments. Low-mass galaxies might have been captured as satellites of more massive galaxies, as they were more affected by local processes and the central galaxies of their systems than by their large-scale environments. Additionally, the lack of assembly time differences at low stellar masses may be understood within the halo occupation distribution paradigm.

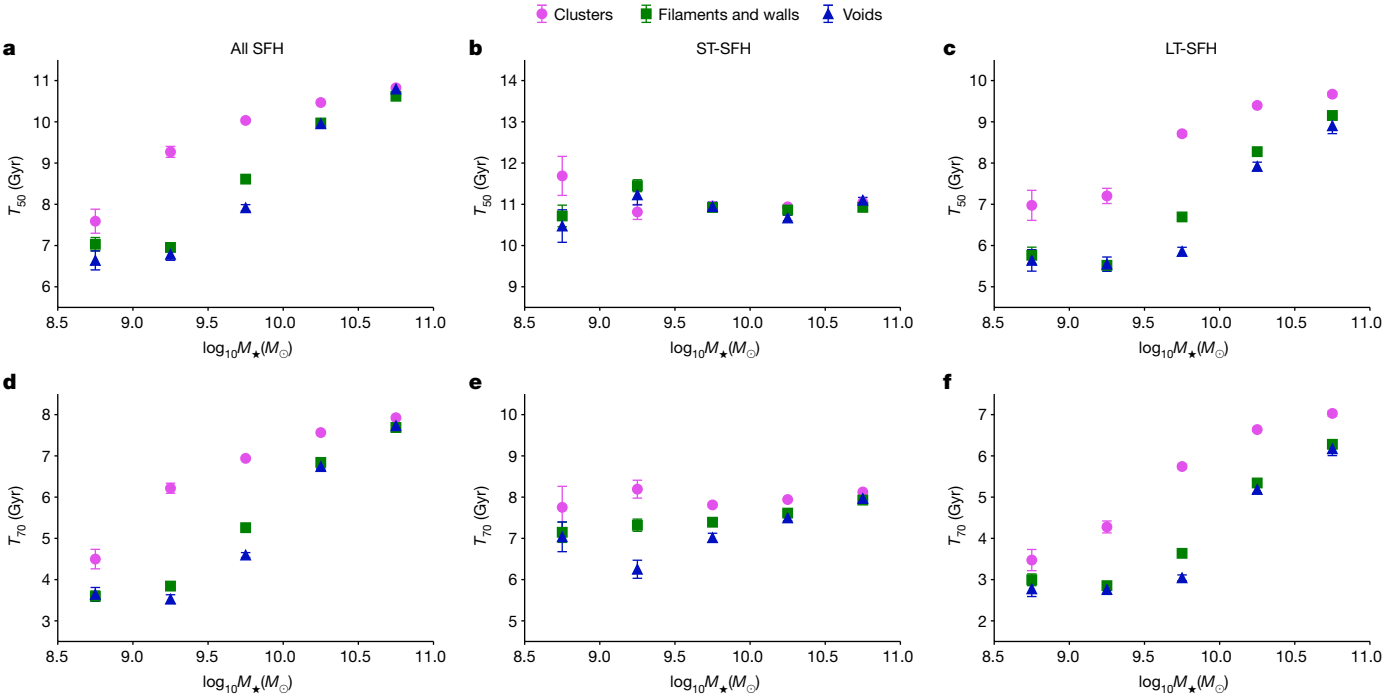

Fig. 4 | Median assembly times versus stellar mass. a–f, Assembly time (Gyr) of 50% (T_{50}) (**a**) and 70% (T_{70}) (**d**) of the stellar mass for all the SFH types, galaxies with ST-SFH (**b** and **e**) and LT-SFH (**c** and **f**), in voids (blue triangles), filaments and walls (green squares) and clusters (purple circles). The samples used take into account the selection criteria applied by the quality control analysis and are based on the same stellar mass distributions inside every stellar mass bin. The error bars represent the standard error of the mean (1σ). The values and errors represented in this figure are shown in Extended Data Table 1, together with the number (and fraction of the SFH types) of galaxies in each large-scale environment and stellar mass bin.

We observe differences in the evolution of galaxies when comparing their SFHs for different large-scale environments, SFH types and stellar masses. Although the mechanics that generate these differences are not clear yet, we can identify several processes that might have triggered these SFH differences between galaxies in different large-scale environments. Differences in the halo-to-stellar mass ratio, the activity of active galactic nuclei (AGNs) and the gas accretion between the three large-scale environments might be some of the reasons why the SFHs in void galaxies are, on average, slower than in filaments and walls and much slower than in clusters (see Methods 'Additional discussion' for a more detailed discussion).

Online content

Any methods, additional references, Nature Portfolio reporting summaries, source data, extended data, supplementary information, acknowledgements, peer review information; details of author contributions and competing interests; and statements of data and code availability are available at https://doi.org/10.1038/s41586-023-06109-1.

1. Peebles, P. J. E. The void phenomenon. *Astrophys. J.* **557**, 495–504 (2001).
2. Kreckel, K. et al. Only the lonely: H I imaging of void galaxies. *Astron. J.* **141**, 4 (2011).
3. Pan, D. C., Vogeley, M. S., Hoyle, F., Choi, Y.-Y. & Park, C. Cosmic voids in Sloan Digital Sky Survey data release 7. *Mon. Not. R. Astron. Soc.* **421**, 926–934 (2012).
4. Varela, J., Betancort-Rijo, J., Trujillo, I. & Ricciardelli, E. The orientation of disk galaxies around large cosmic voids. *Astrophys. J.* **744**, 82 (2012).
5. van de Weygaert, R. Voids and the cosmic web: cosmic depression & spatial complexity. In *Proc. of the International Astronomical Union*, Vol. 308 (eds van de Weygaert, R., Shandarin, S., Saar, E. & Einasto, J.) 493–523 (Cambridge Univ. Press, 2016).
6. Rojas, R. R., Vogeley, M. S., Hoyle, F. & Brinkmann, J. Photometric properties of void galaxies in the Sloan Digital Sky Survey. *Astrophys. J.* **617**, 50–63 (2004).
7. Rojas, R. R., Vogeley, M. S., Hoyle, F. & Brinkmann, J. Spectroscopic properties of void galaxies in the Sloan Digital Sky Survey. *Astrophys. J.* **624**, 571–585 (2005).
8. Patiri, S. G., Prada, F., Holtzman, J., Klypin, A. & Betancort-Rijo, J. The properties of galaxies in voids. *Mon. Not. R. Astron. Soc.* **372**, 1710–1720 (2006).
9. Park, C. et al. Environmental dependence of properties of galaxies in the Sloan Digital Sky Survey. *Astrophys. J.* **658**, 898–916 (2007).
10. Hoyle, F., Vogeley, M. S. & Pan, D. Photometric properties of void galaxies in the Sloan Digital Sky Survey data release 7. *Mon. Not. R. Astron. Soc.* **426**, 3041–3050 (2012).
11. Kreckel, K. et al. The Void Galaxy Survey: optical properties and H I morphology and kinematics. *Astron. J.* **144**, 16 (2012).
12. Ricciardelli, E., Cava, A., Varela, J. & Quilis, V. The star formation activity in cosmic voids. *Mon. Not. R. Astron. Soc.* **445**, 4045–4054 (2014).
13. Beygu, B. et al. The Void Galaxy Survey: star formation properties. *Mon. Not. R. Astron. Soc.* **458**, 394–409 (2016).
14. Florez, J. et al. Void galaxies follow a distinct evolutionary path in the Environmental COntext Catalog. *Astrophys. J.* **906**, 97 (2021).
15. Szomoru, A., van Gorkom, J. H., Gregg, M. D. & Strauss, M. A. An HI survey of the Bootes void. II. The analysis. *Astron. J.* **111**, 2150 (1996).
16. Beygu, B., Kreckel, K., van de Weygaert, R., van der Hulst, J. M. & van Gorkom, J. H. An interacting galaxy system along a filament in a void. *Astron. J.* **145**, 120 (2013).

Methods

Sample selection

Our void galaxy sample is extracted from a nearby void galaxy catalogue defined by the Calar Alto void integral-field treasury survey (CAVITY)[17] project. This Calar Alto Observatory[18] legacy project is generating the first statistically complete integral-field unit (IFU) dataset of void galaxies. The CAVITY survey presents a well-defined selection of void galaxies, which are fully enclosed in the Sloan Digital Sky Survey (SDSS) footprint within a 0.01 and 0.05 redshift range and cover a wide range of stellar masses ($10^{8.5} \leq M_{\star}[M_{\odot}] < 10^{11.0}$). The CAVITY survey aims to observe approximately 300 galaxies with the PMAS-PPAK IFU at the Calar Alto Observatory, along with ancillary deep optical imaging, CO and HI data (I.P. et al., manuscript in preparation) to characterize the spatially resolved stellar populations and ionized gas content of void galaxies, together with their kinematics and dark mass assembly. The CAVITY mother sample, which is made of 2,529 galaxies distributed in 15 voids, is a subsample of a previously defined catalogue of void galaxies presented in ref. 3, where they apply the VoidFinder[19,20] algorithm to the galaxy distribution of the SDSS[21] and identify 79,947 galaxies in 1,055 voids with mean density contrast $\delta\rho/\rho = -0.94 \pm 0.03$ and radii larger than 10 h^{-1} Mpc. The VoidFinder algorithm classifies as potential void galaxies those with their third nearest neighbour distance $d_3 > 6.3\ h^{-1}$ Mpc and removes them from the SDSS galaxy sample, leaving only galaxies in denser large-scale environments. Then, it generates a space grid of cubic cells of size 5 h^{-1} Mpc, identifies the empty ones as potential voids and fits maximal spheres inside these empty regions. Spheres overlapping by more than 10% are unified in the same void and galaxies inside these spheres are classified as void galaxies. The sphere with the same volume as the void defines its effective radius. However, voids are not perfectly spherical and some void galaxies lie beyond the effective radius of their void. There are many algorithms to find voids and other large-scale structures such as filaments, walls and clusters. These algorithms differ in the classification of the galaxies into different large-scale structures, especially when they are very close to the limit of the void, and some galaxies may have been potentially mis-classified as void galaxies. The CAVITY project carries out a selection of galaxies from this catalogue[3] that lie in the inner region of the voids (distance from the centre below 80% of the effective radius of the void) to avoid the possible inclusion of galaxies inhabiting denser environments. Galaxies that satisfy the completeness (at least 20 galaxies distributed along the radius of the void) and observational (15 voids distributed along right ascension for continuous visibility along the year) requirements of the project form part of the CAVITY mother galaxy sample.

The control sample comprises galaxies inhabiting large-scale environments in the nearby Universe that are denser than voids: these are filaments, walls and clusters. We divide it into two different samples: one is made of galaxies in clusters while the other is made of galaxies in filaments and walls. The number density of galaxies is very similar in filaments and walls; therefore, we consider both environments together (filaments and walls hereafter) as the regions where galaxies are neither in voids nor in clusters. We begin the selection with 109,945 objects that are classified in SDSS as galaxies, have available spectral data in the SDSS and lie in the same redshift range as the CAVITY mother galaxy sample (0.01–0.05). We remove 38,473 void galaxies by excluding objects that belong to the previously cited catalogue of void galaxies[3]. We then cross-match the remaining galaxies with a previously defined catalogue of groups of galaxies[22] from SDSS (considering objects with 30 or more companions as cluster galaxies[23]) and separate 6,189 objects, which makes the cluster galaxy control sample. The remaining 65,283 galaxies are considered to be filament and wall galaxies. Furthermore, to save computational time, we select from this sample a random subsample of 15,000 filament and wall galaxies preserving the same $g-r$ colour, stellar mass and redshift distributions (two-sample Kolmogorov–Smirnov (KS)-test P value > 0.95). These three samples are magnitude-limited due to the SDSS completeness limit at r-Petrosian < 17.77 mag (refs. 24,25). This means that the sample is progressively less sensitive to faint objects with increasing redshift. However, given the type of study that we carry out and given the narrow redshift range of the CAVITY sample, we do not expect this to be a severe problem for this work.

In Extended Data Fig. 2, we compare the colour and stellar mass distributions of the three samples. We see that part of the void galaxies are located in the red sequence but they mainly populate the blue cloud. This distribution is more balanced in filaments and walls where galaxies are equally distributed between the red sequence and the blue cloud. However, the majority of cluster galaxies cover the red sequence and only a small part of them are distributed over the blue cloud. As observed before[6–14], void galaxies are, on average, bluer and less massive than galaxies in filaments, walls and clusters. Then, we proceed to carry out our analysis and quality control cuts (see Methods 'Quality control' for more details) to remove some galaxies with badly fitted spectra (mainly low-mass objects from the blue cloud with low signal-to-noise ratio) that modify the distributions (Extended Data Fig. 3). We lose 1,542 (61%) galaxies from voids, 8,537 (57%) from filaments and walls and 2,832 (46%) from clusters. The mean stellar masses of the removed galaxies are similar in the three environments ($10^{9.2\pm0.1}\ M_{\odot}$ in voids, $10^{9.3\pm0.1}\ M_{\odot}$ in filaments and walls and $10^{9.5\pm0.1}\ M_{\odot}$ in clusters). Finally, after this quality control, we are left with 987 galaxies in voids, 6,463 in filaments and walls and 3,357 in clusters for our study. In Extended Data Fig. 3 we compare the colour and stellar mass distribution of the samples after our quality control. These are the samples we use for the global SFH comparison in Figs. 1, 2 and 3.

As seen in Extended Data Figs. 2 and 3, the stellar mass distribution of these samples is not the same even after the quality control. Void galaxies are, on average, less massive than galaxies in denser environments. Therefore, to extend the comparison for a given stellar mass, we define five stellar mass bins (with a 0.5 dex width) between $10^{8.5} M_{\odot}$ and $10^{11.0}\ M_{\odot}$ and we generate two control subsamples with the same stellar mass distribution as our void galaxy sample inside every stellar mass bin. We apply the two-sample KS-test with P values above 0.95 to ensure the accuracy with which the stellar mass distributions are matched. We have not been able to extend the bins at lower or higher stellar masses because the number of galaxies beyond these limits was not enough, in at least one of the environments, to define subsamples with similar stellar mass distributions when applying the KS-test. We are left with 978 void galaxies (we lose nine void galaxies that lie outside the stellar mass bins), 4,800 filament and wall galaxies and 2,570 cluster galaxies. These are the samples that we use in Fig. 4 to compare the assembly times for a given stellar mass.

Spectral analysis

In this study, we recover the stellar line-of-sight velocity distribution (LOSVD) (paying special attention to the recession velocity, V, and the velocity dispersion, σ), the emission lines, the stellar populations and the SFHs of galaxies by fitting stellar spectrum templates to the observed spectrum of the galaxies. For our analysis, we use the synthetic spectral energy distributions for single-age, single-metallicity stellar populations (SSPs) of the extended medium-resolution Isaac Newton Telescope library of empirical spectra (E-MILES[26–29]) as stellar spectrum templates; the observed galaxy spectra already available in the SDSS-DR7 (ref. 21) as data for analysis; penalized pixel-fitting (pPXF[30–32]) as software to recover the stellar LOSVD and the emission lines of the gas; and the stellar content and kinematics from high resolution galactic spectra via maximum a posteriori (STECKMAP[33,34]) as an algorithm with which to recover the stellar populations and SFHs.

The E-MILES[26–29] SSP models are generated using the BaSTI[35] isochrones and Kroupa[36] universal initial mass function (IMF). We expect that a change in the IMF would shift[37] our results (assembly times T_{50} and T_{70}). However, as we assume the same IMF for the three large-scale environments, it will affect our SFHs equally regardless of the environment

and thus relative differences between voids, filaments and walls, and clusters should remain. These models cover a wavelength range from 1,680 Å to 50,000 Å with linear wavelength sampling having a pixel separation of 1.00 Å and a variable instrumental dispersion of full-width at half-maximum (FWHM) between 2.51 Å and 23.57 Å, which is constant (2.51 Å) inside the fitting wavelength range (3,750–5,450 Å) of our analysis.

The SDSS-DR7 (ref. 21) contains integrated optical spectra (fibre aperture with 3 arcsec diameter) for 1.6 million objects, including 930,000 galaxies, 120,000 quasars and 460,000 stars observed at the Apache Point Observatory (APO) 2.5 m telescope. The SDSS spectra have a wavelength coverage from 3,800 Å to 9,200 Å, logarithmic wavelength sampling with a pixel separation of 69 km s^{-1} ($\Delta\log_{10}(\lambda) = 10^{-4}$ dex) and a variable spectral power resolution ranging from $R \approx 1{,}500$ at 3,800 Å to $R \approx 2{,}500$ at 9,000 Å. The instrumental dispersion of the SDSS spectra is variable (FWHM ≈ 2.00–3.00 Å) inside the fitting wavelength range (3,750–5,450 Å) of our analysis and it is different for every galaxy. This is taken into account later in the analysis.

The pPXF[30–32] algorithm implements a non-parametric full-spectral-fitting technique to recover the LOSVD of stars and emission lines. We assume Gaussian–Hermite LOSVD for the stars and a pure Gaussian LOSVD for the emission lines. This algorithm uses stellar and gas spectral templates, chooses a combination of them and convolves them with the LOSVD that better fits the spectrum of the galaxy. We use the E-MILES stellar templates and, for the emission lines, we place several lines in the same template with fixed relative fluxes of emission-line doublets or Balmer series. The E-MILES stellar templates are synthetic or have been observed with instruments that are different from the one used to observe the spectrum of the galaxy. This means that the wavelength sampling and instrumental dispersion of the stellar templates (linear sampling and FWHM = 2.51 Å of instrumental dispersion) are different compared with the spectrum of the galaxy (logarithmic and FWHM ≈ 2.00–3.00 Å). We resample the templates and convolve both the templates and the observed spectra of the galaxies to have the same wavelength sampling (logarithmic) and instrumental dispersion (3.00 Å) in all of them.

The STECKMAP[33,34] algorithm recovers the stellar populations of a galaxy as a combination of SSPs that are fitted to the observed spectrum of the galaxies, after removing the emission lines and assuming fixed stellar LOSVD (both previously derived with pPXF). From this combination of SSPs we derive the stellar mass fraction, metallicity and age of the currently living stars of the galaxy. Afterwards, we apply a correction factor (which depends on the age and metallicity of each stellar population and is provided by the MILES group[38]) to the current stellar mass fractions, so as to take into account the stars that were formed at a given cosmic look-back time but are not alive any more. For this purpose, we follow the prescriptions in refs. 39–41, using BaSTI[35] isochrones and Kroupa[36] IMF. Finally, from these stellar population ages and corrected stellar mass fractions, we derive the SFH of a galaxy, as the cumulative stellar mass fraction formed at a given look-back time, and estimate its errors as the standard deviation of five Monte Carlo solutions of STECKMAP. Additionally, we interpolate over the cumulative SFH to calculate the times when 50% (T_{50}) and 70% (T_{70}) of the stellar mass of the galaxy was formed. We repeat this for the five Monte Carlo solutions and estimate the errors as the standard deviation. Examples of SFHs are shown in Extended Data Fig. 1 for two individual galaxies.

Quality control

After applying this analysis to our samples of galaxies in voids (2,545 objects), filaments and walls (15,000) and clusters (6,189), we carry out a quality control to identify and remove the badly fitted spectra. There are two main aspects that affect the fit quality: the signal-to-noise ratio of the spectra and the intensity of the emission lines. The fit residual, which is the difference between the observed and the fitted spectrum, is a good indicator of the fit quality. A high fit residual means that the observed spectrum is noisy or the fitted spectrum does not match the real one. In Extended Data Fig. 4a, we show the standard deviation of the fit residual normalized by the level of continuum around Hβ (the second emission line of the Balmer series of the hydrogen atom, σ_{res}(Hβ)/cont.) versus the signal-to-noise ratio in the continuum. The equivalent width of Hβ ($\Delta H\beta_{eq}$) is colour coded. Here, we see how the fit quality (stellar and gas emission) is affected by the signal-to-noise ratio. The level of fit residual, relative to the continuum, decreases with signal-to-noise ratio. We considered that a signal-to-noise ratio greater than or equal to 20 provides a good quality fit with a level of residual lower than 2% of the continuum for the great majority of the galaxies. However, there is a group of galaxies with really intense or wide emission lines that are not well fitted although they have high signal-to-noise ratio.

The pPXF algorithm is not efficient at fitting very intense or non-Gaussian emission lines and may generate high fit residuals. These residuals are small compared with the continuum (below 2%) in bright galaxies but may be higher than the level of noise, leaving wavy features in the spectrum that may affect the fit of stellar populations. In Extended Data Fig. 4b, we show residual-to-noise ratio as the standard deviation of the residual at Hβ normalized by standard deviation of noise in the continuum next to Hβ (σ_{res}(Hβ)/σ_{noise}(Hβ)) versus the signal-to-noise ratio in the continuum; $\Delta H\beta_{eq}$ is colour coded. Here, we see that some bright galaxies (with intense emission lines, in general) have the level of residual much higher than the level of noise. After a visual inspection of a set of these galaxies, we find featured residuals due to asymmetrical, wide, or non-Gaussian emission lines (see good and bad fit examples in Extended Data Fig. 5) and consider that $\sigma_{res}(H\beta)/\sigma_{noise}(H\beta) \leq 2.0$ provides a good quality fit. However, this is only a small fraction of the total number of galaxies (5% in voids, 8% in filaments and walls and 7% in clusters).

Additionally, as final step in our quality control, we take into account the aperture effect in the SDSS spectra. The optical spectra are available for the central region of our galaxies (fibre aperture with 3 arcsec diameter). This might introduce a bias for samples covering a large redshift range where this aperture would cover only the inner region of the nearby objects but a large fraction of the galaxy for the distant ones. However, the apparent radius distribution (Extended Data Fig. 6) is similar for the three samples and the redshift range (0.01 to 0.05) is the same, with absolute apertures ranging from 0.3 kpc to 1.6 kpc. We remove from our samples any galaxies with $R_{90r} > 20$ arcsec, for which the aperture effect would have a larger influence, to minimize a possible size bias in our study. The aperture effect affects our study only in the sense that our results are valid for the centre of the galaxy only.

Additional discussion

In Fig. 2, we show that the SFH of a galaxy can be classified as ST-SFH or LT-SFH. Although it might be tempting to associate the SFH bimodality with the current galaxy colour, morphology or local environment, the SFH types do not correspond to the bimodal colour or morphology distributions (Extended Data Fig. 7) and they do not strongly correlate with the local density. The SFH type determines the evolution of a galaxy, in general, along its entire life. However, the colour and morphology are associated with current properties of the galaxy, which should not be that strongly affected by the overall SFH type (shape) but by the most recent stages of the SFH, the current environmental state or physical conditions (gas content, interactions, accretion, etc.)

Additionally, in Fig. 4c,f, we do not find assembly time differences for low-mass galaxies. This observation can be interpreted based on the halo occupation distribution paradigm, as mentioned in the main text. According to this paradigm, galaxies in voids have higher halo mass (approximately 10%)[42] than in denser environments for a given stellar mass. This, together with the lower probability of finding high-mass galaxies in voids, makes low-mass galaxies in voids more likely to be the central objects of a system. However, low-mass galaxies in voids, which would have presumably evolved more slowly than galaxies in

filaments and walls due to their large-scale environment, might have compensated for these SFH differences by accelerating their star formation owing to their higher halo masses.

Our main finding is that galaxies assemble their stellar mass in voids more slowly than in filaments and walls and much more slowly than in clusters (Fig. 4). We discuss some of the physical processes that might have triggered these differences. Previous cosmological simulation analyses[42–45] find that the halo-to-stellar mass ratio is higher in void galaxies compared with galaxies in denser large-scale environments, which suggests that galaxies in voids evolve more slowly than in filaments, walls and clusters. Regarding the effect of AGNs, some observational studies find statistical evidence for a larger fraction of AGNs[46,47] and massive black holes[47] in voids. However, these differences in the fraction of AGNs between galaxies in voids and in denser environments are not present in other observational studies[48]. No differences in the black hole-to-galaxy mass ratio are reported by other simulation analyses[44]. There is no agreement on how the large-scale environment affects the nuclear activity of the galaxies and it is controversial to consider AGNs as a possible mechanism that triggered the SFH differences that we find. A simulation analysis[49] found that there are mainly two modes of gas accretion in galaxies. In the cold accretion mode, the gas flows along the filaments into the galaxy. This dominates in low-density large-scale environments, low-stellar-mass galaxies and at high redshifts. In the hot accretion mode, the virialized gas around the galaxy falls into it while it cools down. This dominates in cluster large-scale environments, massive galaxies and at low redshifts. This suggests that the gas accretion has been different throughout the SFH between galaxies in voids and denser large-scale environments and this might have introduced current gas content differences between them. Some other observational studies[14,15] do not find any atomic gas mass differences between voids and galaxies in denser large-scale environments although others[11,45,50] find a tentative lack of atomic gas in void galaxies at stellar masses above $10^{9.5}\,M_{\odot}$, which is the same range in which we find the LT-SFH differences. However, a lack of atomic gas in galaxies does not necessarily imply a lack of molecular gas[50–55] from which the stars are formed.

Data availability

The analysis and results in this work are based on public data: SDSS query/CasJobs (http://casjobs.sdss.org/casjobs/) and SDSS spectra (http://data.sdss.org/sas/dr16/sdss/spectro/redux/26/spectra/). Interested researchers can reproduce our analysis following the steps in the Methods section and using the public data and codes. They can also compare with our results using the electronic spreadsheets associated with the figures in the main text. We do not place our results for individual galaxies into public repository at the moment because two PhD students inside the CAVITY project are using these results for their thesis. Additionally, a great effort has been required to carry out this analysis and the CAVITY project plans to base many of their future works on these results. At a later stage, once the PhD projects are finished and convenient exploitation of the work within the collaboration is done, we plan to make an ample dataset available for the community. We need to highlight the 'legacy' nature of this project, as agreed in the memorandum of understanding with the Calar Alto observatory, but, first, we reserve our rights for an embargo period for the full exploitation of this project. Source data are provided with this paper.

Code availability

Codes that support the analysis in this study are publicly available: pPXF[30–32] (https://www-astro.physics.ox.ac.uk/~cappellari/software/) and STECKMAP[33,34] (https://urldefense.com/v3/_https://github.com/pocvirk/STECKMAP_;!!D9dNQwwGXtA!VggZnNu4_e840FF17iVF0CW79nTSLkzJ53o14bQwryoS3l_alwG4PzL_OFaVMnHJ8UNWkXs5WYNJtvkFBU-3y7O2nofr$).

17. Calar Alto void integral-field treasury survey. *CAVITY* https://cavity.caha.es/.
18. Calar Alto Observatory. *CAHA* https://www.caha.es/.
19. El-Ad, H. & Piran, T. Voids in the large-scale structure. *Astrophys. J.* **491**, 421–435 (1997).
20. Hoyle, F. & Vogeley, M. S. Voids in the Point Source Catalogue Survey and the Updated Zwicky Catalog. *Astrophys. J.* **566**, 641–651 (2002).
21. Abazajian, K. N. et al. The seventh data release of the Sloan Digital Sky Survey. *ApJS* **182**, 543–558 (2009).
22. Tempel, E., Tuvikene, T., Kipper, R. & Libeskind, N. I. Merging groups and clusters of galaxies from the SDSS data. The catalogue of groups and potentially merging systems. *Astron. Astrophys.* **602**, 100 (2017).
23. Abell, G. O., Corwin, HaroldJ.,G. & Olowin, R. P. A catalog of rich clusters of galaxies. *ApJS* **70**, 1 (1989).
24. Strauss, M. A. et al. Spectroscopic target selection in the Sloan Digital Sky Survey: the main galaxy sample. *Astron. J.* **124**, 1810–1824 (2002).
25. Argudo-Fernández, M. et al. Catalogues of isolated galaxies, isolated pairs, and isolated triplets in the local Universe. *Astron. Astrophys.* **578**, 110 (2015).
26. Sánchez-Blázquez, P. et al. Medium-resolution Isaac Newton Telescope library of empirical spectra. *Mon. Not. R. Astron. Soc.* **371**, 703–718 (2006).
27. Falcón-Barroso, J. et al. An updated MILES stellar library and stellar population models. *Astron. Astrophys.* **532**, 95 (2011).
28. Vazdekis, A. et al. Evolutionary stellar population synthesis with MILES – II. Scaled-solar and α-enhanced models. *Mon. Not. R. Astron. Soc.* **449**, 1177–1214 (2015).
29. Vazdekis, A., Koleva, M., Ricciardelli, E., Röck, B. & Falcón-Barroso, J. UV-extended E-MILES stellar population models: young components in massive early-type galaxies. *Mon. Not. R. Astron. Soc.* **463**, 3409–3436 (2016).
30. Cappellari, M. & Emsellem, E. Parametric recovery of line-of-sight velocity distributions from absorption-line spectra of galaxies via penalized likelihood. *PASP* **116**, 138–147 (2004).
31. Cappellari, M. Improving the full spectrum fitting method: accurate convolution with Gauss–Hermite functions. *Mon. Not. R. Astron. Soc.* **466**, 798–811 (2017).
32. Cappellari, M. Full spectrum fitting with photometry in ppxf: non-parametric star formation history, metallicity and the quenching boundary from 3200 LEGA-C galaxies at redshift $z\approx0.8$. Preprint at https://doi.org/10.48550/arXiv.2208.14974 (2022).
33. Ocvirk, P., Pichon, C., Lançon, A. & Thiébaut, E. STECMAP: STEllar Content from high-resolution galactic spectra via Maximum A Posteriori. *Mon. Not. R. Astron. Soc.* **365**, 46–73 (2006).
34. Ocvirk, P., Pichon, C., Lançon, A. & Thiébaut, E. STECKMAP: STEllar Content and Kinematics from high resolution galactic spectra via Maximum A Posteriori. *Mon. Not. R. Astron. Soc.* **365**, 74–84 (2006).
35. Pietrinferni, A., Cassisi, S., Salaris, M. & Castelli, F. A large stellar evolution database for population synthesis studies. I. Scaled solar models and isochrones. *Astrophys. J.* **612**, 168–190 (2004).
36. Kroupa, P. On the variation of the initial mass function. *Mon. Not. R. Astron. Soc.* **322**, 231–246 (2001).
37. García-Benito, R. et al. Spatially resolved mass-to-light from the CALIFA survey. Mass-to-light ratio vs. color relations. *Astron. Astrophys.* **621**, 120 (2019).
38. Photometric predictions. *MILES* http://research.iac.es/proyecto/miles/pages/predicted-masses-and-photometric-observables-based-on-photometric-libraries.php.
39. Vazdekis, A., Casuso, E., Peletier, R. F. & Beckman, J. E. A new chemo-evolutionary population synthesis model for early-type galaxies. I. Theoretical basis. *ApJS* **106**, 307 (1996).
40. Blakeslee, J. P., Vazdekis, A. & Ajhar, E. A. Stellar populations and surface brightness fluctuations: new observations and models. *Mon. Not. R. Astron. Soc.* **320**, 193–216 (2001).
41. Vazdekis, A. et al. Evolutionary stellar population synthesis with MILES – I. The base models and a new line index system. *Mon. Not. R. Astron. Soc.* **404**, 1639–1671 (2010).
42. Alfaro, I. G., Rodriguez, F., Ruiz, A. N. & Lambas, D. G. How galaxies populate haloes in very low-density environments. An analysis of the halo occupation distribution in cosmic voids. *Astron. Astrophys.* **638**, 60 (2020).
43. Artale, M. C., Zehavi, I., Contreras, S. & Norberg, P. The impact of assembly bias on the halo occupation in hydrodynamical simulations. *Mon. Not. R. Astron. Soc.* **480**, 3978–3992 (2018).
44. Habouzit, M. et al. Properties of simulated galaxies and supermassive black holes in cosmic voids. *Mon. Not. R. Astron. Soc.* **493**, 899–921 (2020).
45. Rosas-Guevara, Y., Tissera, P., Lagos, Cd. P., Paillas, E. & Padilla, N. Revealing the properties of void galaxies and their assembly using the EAGLE simulation. *Mon. Not. R. Astron. Soc.* **517**, 712–731 (2022).
46. Constantin, A., Hoyle, F. & Vogeley, M. S. Active galactic nuclei in void regions. *Astrophys. J.* **673**, 715–729 (2008).
47. Ceccarelli, L., Duplancic, F. & Garcia Lambas, D. The impact of void environment on AGN. *Mon. Not. R. Astron. Soc.* **509**, 1805–1819 (2022).
48. Amiri, A., Tavasoli, S. & De Zotti, G. Role of environment on nuclear activity. *Astrophys. J.* **874**, 140 (2019).
49. Kereš, D., Katz, N., Weinberg, D. H. & Davé, R. How do galaxies get their gas? *Mon. Not. R. Astron. Soc.* **363**, 2–28 (2005).
50. Domínguez-Gómez, J. et al. CO-CAVITY pilot survey: molecular gas and star formation in void galaxies. *Astron. Astrophys.* **658**, 124 (2022).
51. Kenney, J. D. & Young, J. S. CO in H I-deficient Virgo cluster spiral galaxies. *Astrophys. J.* **301**, 13 (1986).
52. Sage, L. J., Weistrop, D., Cruzen, S. & Kompe, C. Molecular gas and star formation within galaxies in the Bootes Void. *Astron. J.* **114**, 1753 (1997).
53. Das, M., Saito, T., Iono, D., Honey, M. & Ramya, S. Detection of molecular gas in void galaxies: implications for star formation in isolated environments. *Astrophys. J.* **815**, 40 (2015).
54. Cortese, L. et al. The selective effect of environment on the atomic and molecular gas-to-dust ratio of nearby galaxies in the Herschel Reference Survey. *Mon. Not. R. Astron. Soc.* **459**, 3574–3584 (2016).

55. Grossi, M. et al. Star-forming dwarf galaxies in the Virgo cluster: the link between molecular gas, atomic gas, and dust. *Astron. Astrophys.* **590**, 27 (2016).
56. Ahumada, R. et al. The 16th data release of the Sloan Digital Sky Surveys: first release from the APOGEE-2 Southern Survey and full release of eBOSS spectra. *ApJS* **249**, 3 (2020).
57. Domínguez Sánchez, H., Huertas-Company, M., Bernardi, M., Tuccillo, D. & Fischer, J. L. Improving galaxy morphologies for SDSS with Deep Learning. *Mon. Not. R. Astron. Soc.* **476**, 3661–3676 (2018).

Acknowledgements We are grateful to the referees who have helped us to improve the readability and clarity of the text. We acknowledge financial support by the research projects AYA2017-84897-P, PID2020-113689GB-I00 and PID2020-114414GB-I00, financed by MCIN/AEI/10.13039/501100011033, the project A-FQM-510-UGR20 financed from FEDER/Junta de Andalucía-Consejería de Transforamción Económica, Industria, Conocimiento y Universidades/Proyecto and by the grants P20_00334 and FQM108, financed by the Junta de Andalucía (Spain). T.R.L. acknowledges support from Juan de la Cierva fellowship (IJC2020-043742-I), financed by MCIN/AEI/10.13039/501100011033. H.C. acknowledges support from the Institut Universitaire de France and the CNES. This work was supported by the Arqus European University and ANR program France 2030. L.S.M. acknowledges support from Juan de la Cierva fellowship (IJC2019-041527-I) financed by MCIN/AEI/10.13039/501100011033. J.F.B. acknowledges support through the RAVET project by the grant PID2019-107427GB-C32 from the Spanish Ministry of Science, Innovation and Universities (MCIU) and through the IAC project TRACES, which is partially supported through the state budget and the regional budget of the Consejería de Economía, Industria, Comercio y Conocimiento of the Canary Islands Autonomous Community. D.E. acknowledges support from a Beatriz Galindo senior fellowship (BG20/00224) from the Spanish Ministry of Science and Innovation. M.A.F. acknowledges support the Emergia program (EMERGIA20_38888) from Consejería de Transformación Económica, Industria, Conocimiento y Universidades and University of Granada. R.G.B. acknowledges financial support from the grants CEX2021-001131-S funded by MCIN/AEI/10.13039/501100011033, SEV-2017-0709 to PID2019-109067-GB100 and grant 202250I003 'AYUDAS DE INCORPORACIÓN A CIENTÍFICOS TITULARES'. S.D.P. acknowledges financial support from Juan de la Cierva Formación fellowship (FJC2021-047523-I) financed by MCIN/AEI/10.13039/501100011033 and by the European Union 'NextGenerationEU'/PRTR, Ministerio de Economía y Competitividad under grant PID2019-107408GB-C44 from Junta de Andalucía Excellence Project P18-FR-2664 and also from the State Agency for Research of the Spanish MCIU through the 'Center of Excellence Severo Ochoa' award for the Instituto de Astrofísica de Andalucía (SEV-2017-0709). G.B.-C. acknowledges financial support from grants PID2020-114461GB-I00 and CEX2021-001131-S, funded by MCIN/AEI/10.13039/501100011033, from Junta de Andalucía (Spain) grant P20-00880 (FEDER, EU) and from grant PRE2018-086111 funded by MCIN/AEI/10.13039/501100011033 and by 'ESF Investing in your future'. K.K. acknowledges funding from the Deutsche Forschungsgemeinschaft (DFG, German Research Foundation) in the form of an Emmy Noether Research Group (grant number KR4598/2-1, PI Kreckel). This research made use of Astropy, a community-developed core Python (http://www.python.org) package for astronomy; ipython; matplotlib; SciPy, a collection of open-source software for scientific computing in Python; APLpy, an open-source plotting package for Python; and NumPy, a structure for efficient numerical computation.

Author contributions J.D.G. is the corresponding author and was involved in sample selection, control sample selection, data analysis, results interpretation and writing. I.P. was involved in sample selection, control sample selection, data analysis, results interpretation and writing. T.R.L. was involved in data analysis, results interpretation and writing. R.F.P. was involved in data analysis, results interpretation and writing. P.S.B. was involved in data analysis, results interpretation and writing. U.L. was involved in sample selection, control sample selection, data analysis, results interpretation and writing. J.F.B. was involved in data analysis, results interpretation and writing. M.A.L. was involved in sample selection, results interpretation and writing. M.A.F. was involved in sample selection, results interpretation and writing. G.B.C. was involved in sample selection, results interpretation and writing. H.C. was involved in results interpretation and writing. S.D.P. was involved in sample selection, control sample selection, results interpretation and writing. D.E. was involved in results interpretation and writing. E.F. was involved in sample selection, results interpretation and writing. R.G.B. was involved in results interpretation and writing. A.J. was involved in results interpretation and writing. K.K. was involved in results interpretation and writing. M.R. was involved in sample selection, results interpretation and writing. L.S.M. was involved in results interpretation and writing. T.H. was involved in results interpretation and writing. R.W. was involved in results interpretation and writing. S.V. was involved in sample selection, control sample selection, results interpretation and writing. A.Z. was involved in sample selection, results interpretation and writing.

Competing interests The authors declare no competing interests.

Additional information
Supplementary information The online version contains supplementary material available at https://doi.org/10.1038/s41586-023-06109-1.
Correspondence and requests for materials should be addressed to Jesús Domínguez-Gómez.
Peer review information *Nature* thanks the anonymous reviewers for their contribution to the peer review of this work. Peer reviewer reports are available.

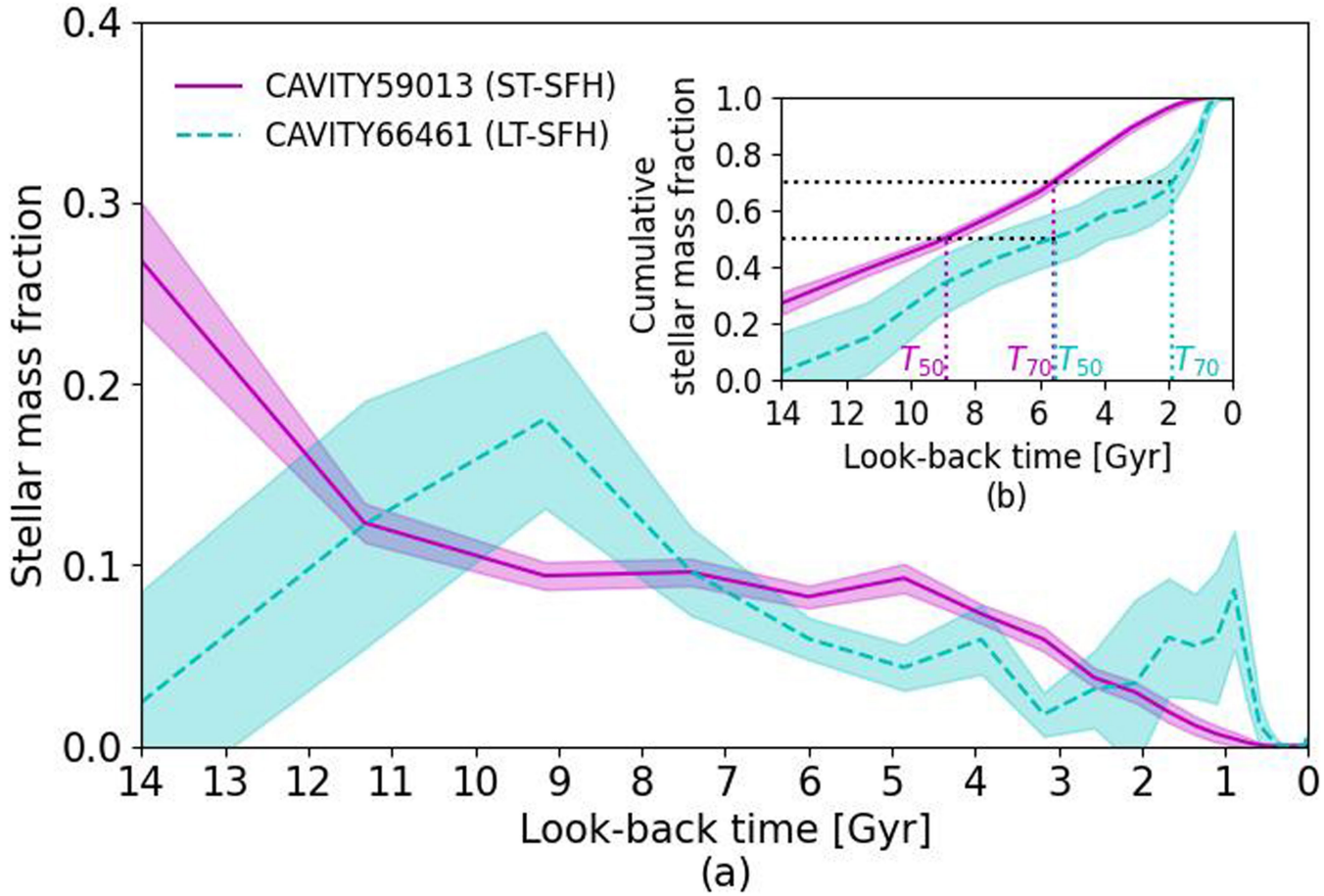

Extended Data Fig. 1 | Examples of star formation histories. a, SFHs and **b**, cumulative SFHs for galaxies CAVITY59013 (solid magenta line) and CAVITY66461 (dashed cyan line), which have ST-SFH and LT-SFH types, respectively. The shaded regions represent the errors of the stellar mass fraction of the SFH. The dotted lines in **b** represent the assembly times of the 50% (T_{50}) and 70% (T_{70}) of the stellar mass.

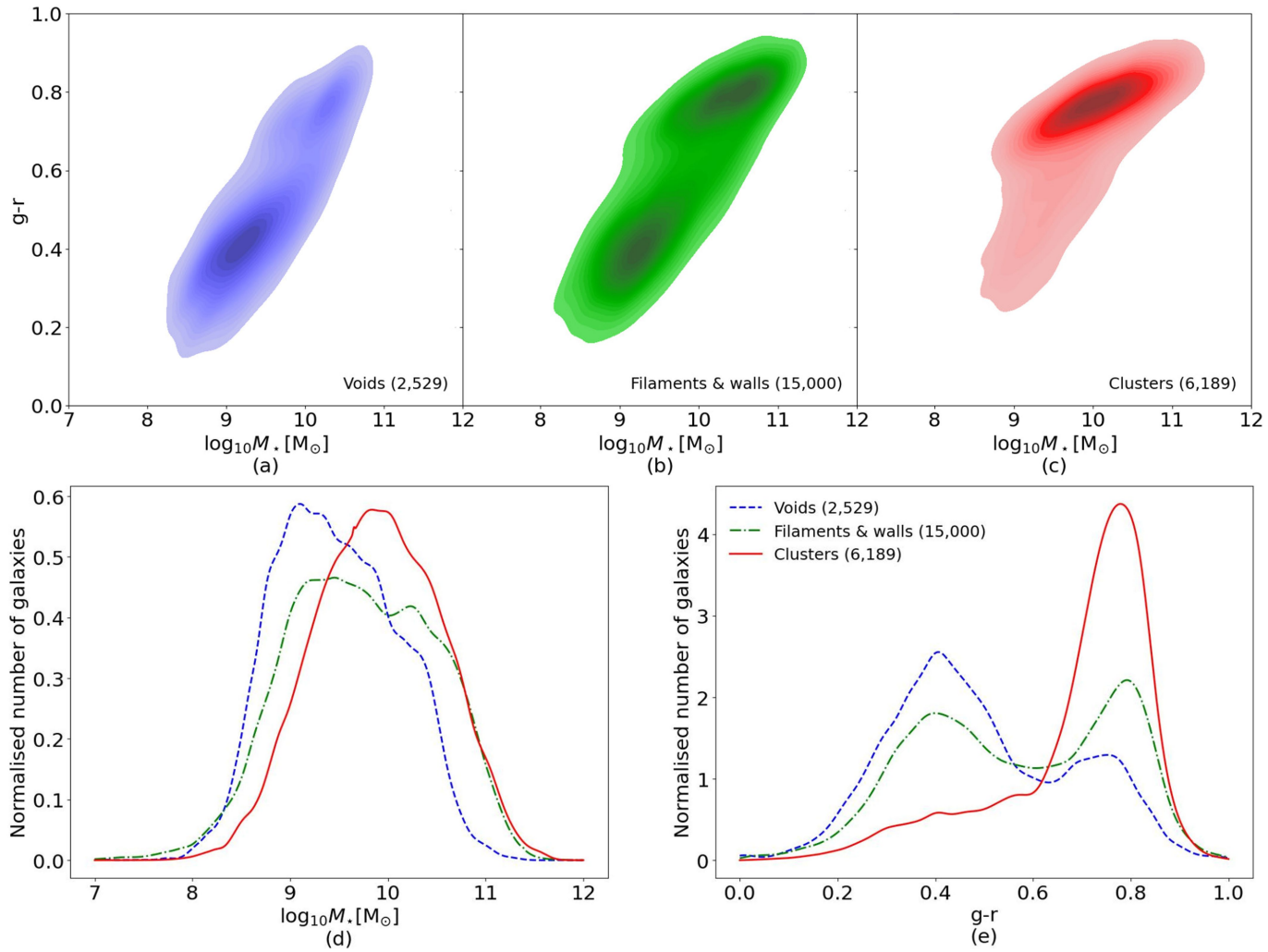

Extended Data Fig. 2 | Colour and stellar mass distribution before the quality control. a–**c**, Colour versus stellar mass diagram for galaxies in voids (**a**), filaments (**b**), and clusters (**c**). **d**,**e**, Normalized distributions of the stellar mass (**d**) and $g-r$ colour (**e**) for galaxies in voids (blue dashed line), filaments and walls (green dot-dashed line), and clusters (red solid line).

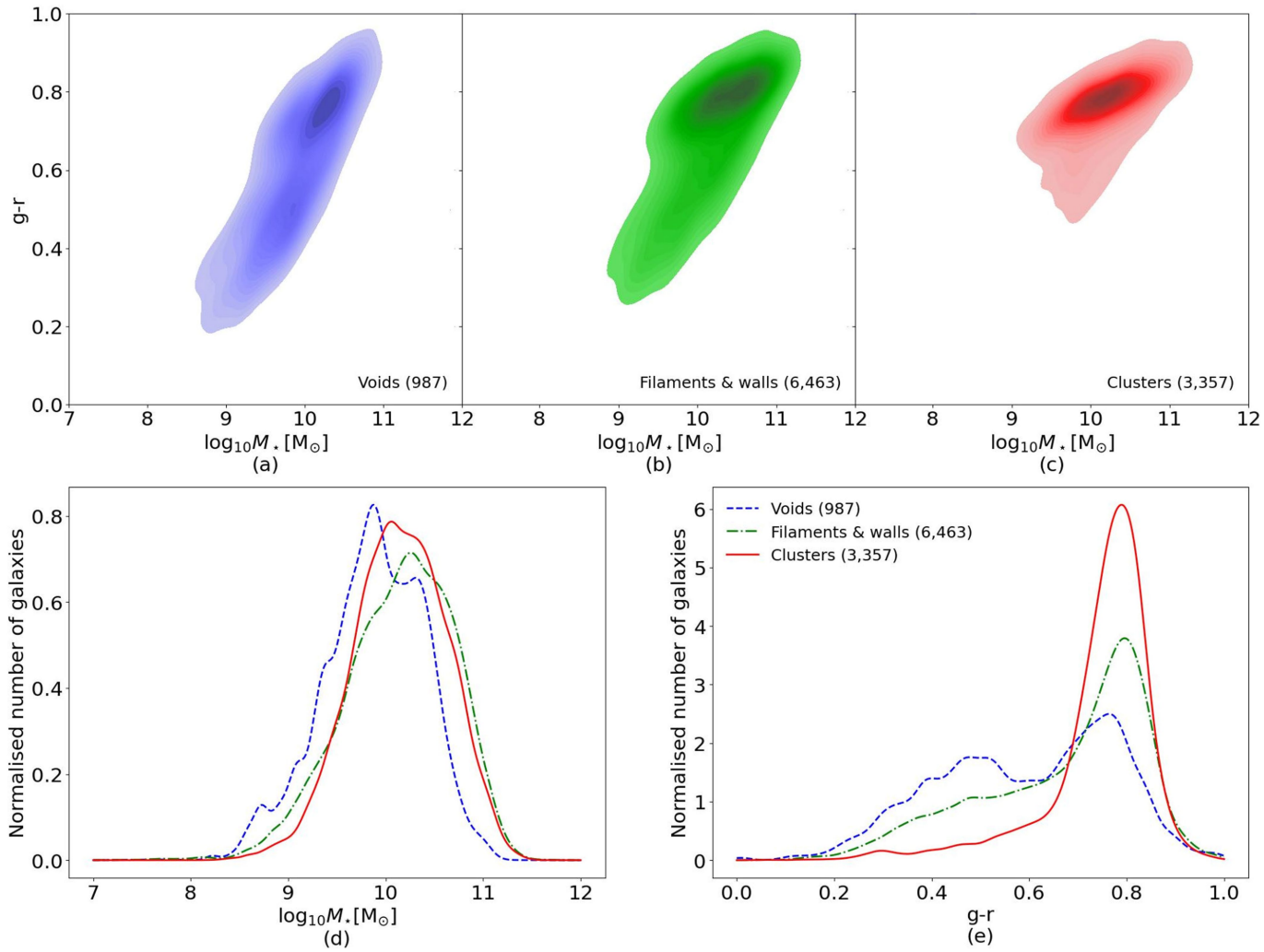

Extended Data Fig. 3 | Colour and stellar mass distribution after the quality control. a–**c**, Colour versus stellar mass diagram for galaxies in voids (**a**), filaments (**b**), and clusters (**c**). **d**,**e**, Normalized distributions of the stellar mass (**d**) and $g-r$ colour (**e**) for galaxies in voids (blue dashed line), filaments and walls (green dot-dashed line), and clusters (red solid line).

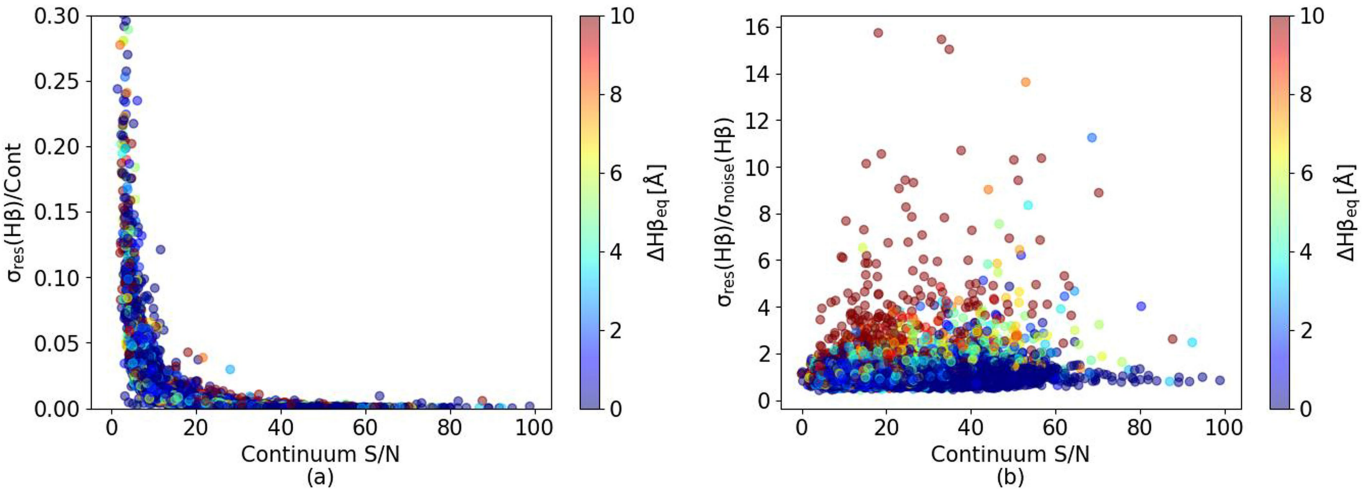

Extended Data Fig. 4 | Fit residuals versus spectral signal-to-noise, and emission lines. a, Standard deviation of the spectral fit residual (σ_{res}(Hβ)) normalized by the level of the continuum (Cont) around Hβ versus the spectral signal-to-noise (S/N) ratio in the continuum. **b**, Residual-to-noise ratio as (σ_{res}(Hβ)) normalized by standard deviation of noise in the continuum next to Hβ (σ_{noise}(Hβ)) versus the S/N in the continuum. The Hβ equivalent with (ΔHβ_{eq}) is colour-coded in both panels.

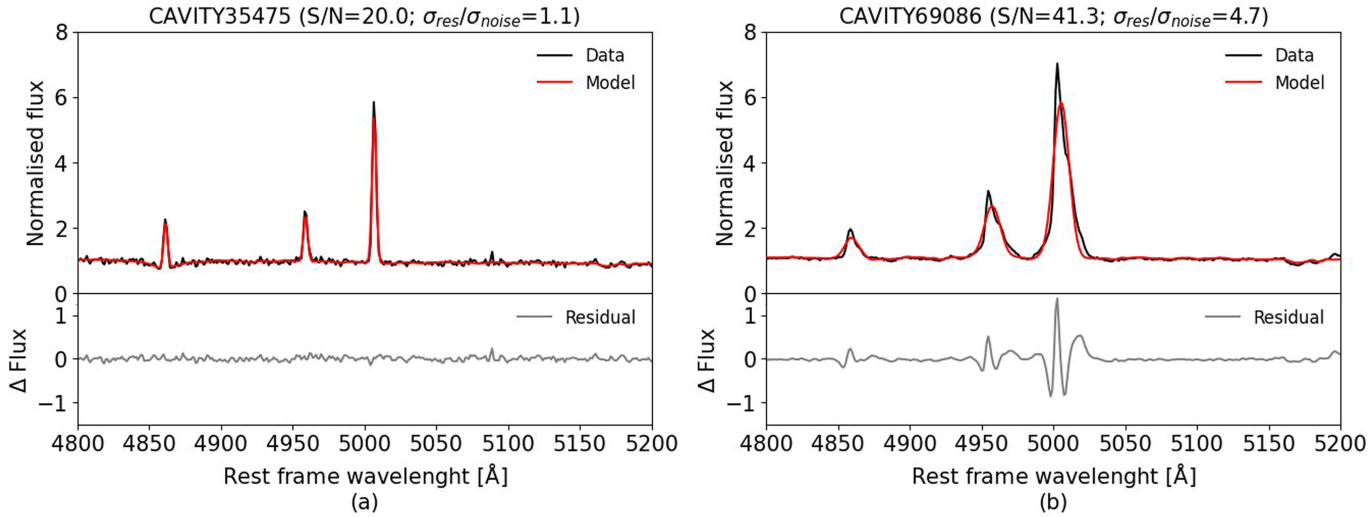

Extended Data Fig. 5 | Examples of pPXF spectral fit of emission lines. **a**, Good fit example of a galaxy with signal-to-noise ratio of S/N = 20.0 and residual-to-noise ratio of $\sigma_{res}/\sigma_{noise} = 1.1$. **b**, Bad fit example of a galaxy with S/N = 41.3 and $\sigma_{res}/\sigma_{noise} = 4.7$. The black and red lines represent the observed and the fitted spectrum of the galaxy, respectively. The grey lines represent the fit residuals.

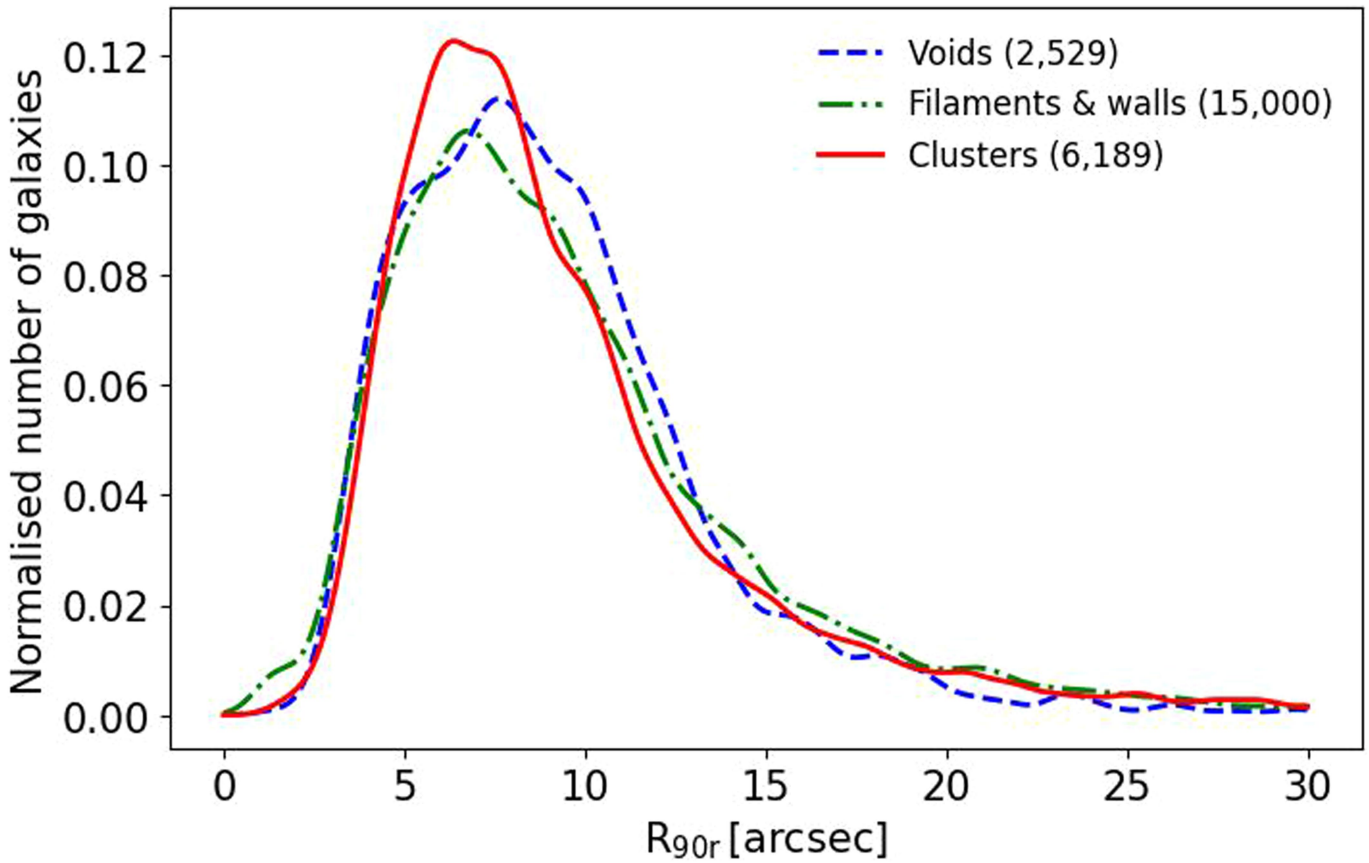

Extended Data Fig. 6 | Distribution of apparent radius. Normalized number of galaxies as a function of the apparent radius (R_{90r} from SDSS) for galaxies in voids (blue dashed line), filaments and walls (green dot-dashed line), and clusters (red solid line) before the quality control. The apparent radius of the galaxies is represented by the petrosian radius containing the 90% of the total flux of the galaxy in r band (SDSS[56]).

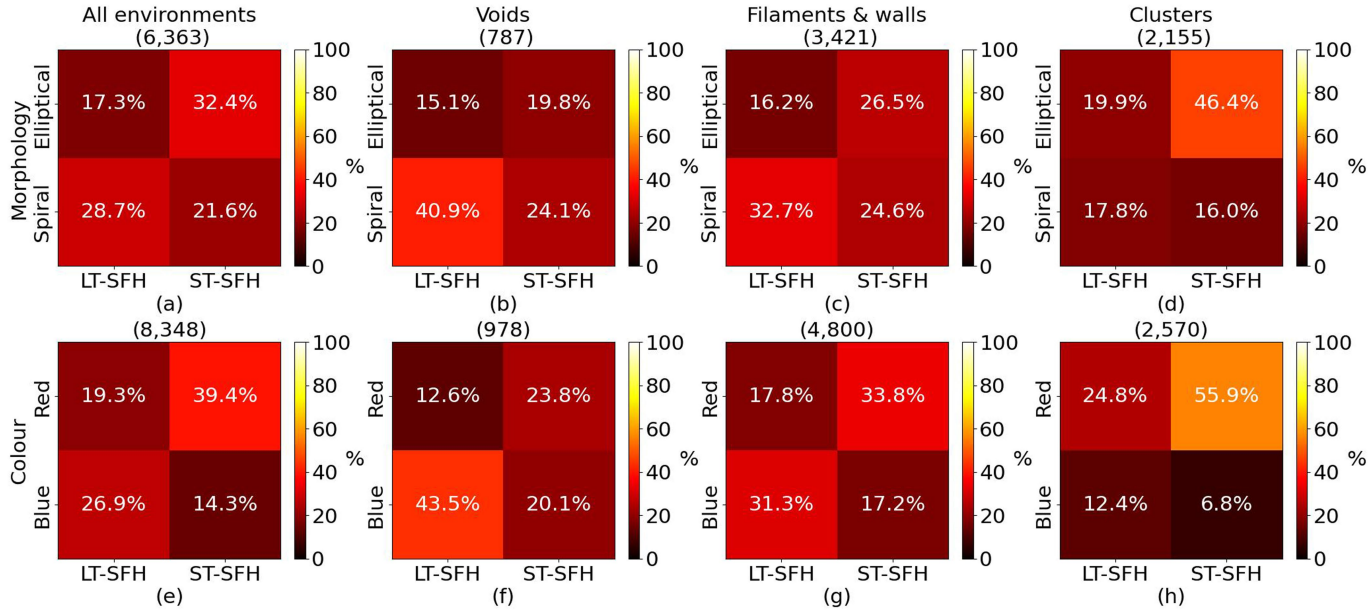

Extended Data Fig. 7 | Correlation between the star formation history type, current morphology and colour of the galaxy. a–**h**, Fraction of spiral and elliptical galaxies, or blue and red galaxies with LT-SFH and ST-SFH types is shown for all the environments together (**a**,**e**), for voids (**b**,**f**), filaments and walls (**c**,**g**), and clusters (**d**,**h**), with the same stellar mass distribution. The number of galaxies is shown between brackets over each panel. Galaxies are blue if their $g-r<0.7$, red if $g-r>0.7$, spiral if T-type >0[57], and elliptical if T-type <0. Galaxies with ST-SFH are more likely to be elliptical or red. On the contrary, galaxies with LT-SFH are more likely to be spiral or blue. However, there is a significant fraction galaxies with ST-SFHs that are blue or spiral, and galaxies with LT-SFHs that are red or elliptical.

Extended Data Table 1 | Median assembly times

$\log_{10} M_\star[M_\odot]$	Voids n(%)	Voids T_{50} [Gyr]	Voids T_{70} [Gyr]	Filaments & walls n(%)	Filaments & walls T_{50} [Gyr]	Filaments & walls T_{70} [Gyr]	Clusters n(%)	Clusters T_{50} [Gyr]	Clusters T_{70} [Gyr]
(a) All SFH									
8.5-9.0	56	6.64±0.23	3.64±0.17	105	7.03±0.16	3.60±0.12	30	7.59±0.29	4.50±0.24
9.0-9.5	159	6.79±0.14	3.53±0.11	326	6.95±0.09	3.84±0.07	100	9.27±0.13	6.22±0.12
9.5-10.0	363	7.92±0.08	4.60±0.06	1500	8.61±0.04	5.26±0.03	855	10.03±0.04	6.94±0.04
10.0-10.5	309	9.95±0.06	6.74±0.05	2199	9.97±0.02	6.84±0.02	1212	10.47±0.02	7.57±0.02
10.5-11.0	91	10.79±0.07	7.73±0.07	670	10.62±0.03	7.69±0.03	373	10.82±0.03	7.93±0.03
(b) ST-SFH									
8.5-9.0	8(14%)	10.47±0.39	7.04±0.36	24(23%)	10.72±0.26	7.15±0.25	9(30%)	11.69±0.47	7.75±0.51
9.0-9.5	40(25%)	11.23±0.24	6.25±0.22	80(25%)	11.45±0.14	7.32±0.15	39(39%)	10.81±0.18	8.19±0.22
9.5-10.0	127(35%)	10.94±0.11	7.02±0.11	602(40%)	10.92±0.05	7.39±0.05	463(54%)	10.96±0.05	7.81±0.05
10.0-10.5	187(61%)	10.67±0.07	7.50±0.07	1263(57%)	10.86±0.03	7.61±0.03	820(68%)	10.94±0.03	7.94±0.03
10.5-11.0	68(75%)	11.10±0.07	7.97±0.08	476(71%)	10.93±0.03	7.93±0.03	282(76%)	11.05±0.03	8.12±0.03
(c) LT-SFH									
8.5-9.0	48(86%)	5.64±0.26	2.77±0.19	81(77%)	5.76±0.20	3.00±0.14	21(70%)	6.97±0.36	3.47±0.26
9.0-9.5	119(75%)	5.55±0.17	2.76±0.12	246(75%)	5.52±0.11	2.85±0.08	61(61%)	7.20±0.18	4.28±0.14
9.5-10.0	236(65%)	5.86±0.10	3.04±0.07	898(60%)	6.69±0.05	3.64±0.04	392(46%)	8.71±0.06	5.74±0.05
10.0-10.5	122(39%)	7.92±0.10	5.19±0.08	936(43%)	8.28±0.04	5.34±0.03	392(32%)	9.40±0.04	6.64±0.04
10.5-11.0	23(25%)	8.90±0.19	6.17±0.16	194(29%)	9.15±0.06	6.28±0.05	91(24%)	9.67±0.06	7.03±0.07

Assembly time (in Giga years, Gyr) of 50% (T_{50}) and 70% (T_{70}) of the stellar mass for all the SFH types (a), galaxies with ST-SFH (b), and LT-SFH (c), in voids, filaments and walls, and clusters. The used samples take into account the selection criteria applied by the quality control analysis and are based on the same stellar mass distributions inside every stellar mass bin. The error represent the s.e.m. (1σ). The number of galaxies (n) in each environment and stellar mass bin is shown together with the fraction (%) of each SFH type inside every stellar mass bin and environment. These are the values represented in Fig. 4.